

INSTRUMENTS AND METHODS OF INVESTIGATION

PACS numbers: 64.60.ah, **71.30.+h, 75.47.–m**

Scaling of anomalous Hall effect as a method to determine percolation threshold and metal–insulator transition in magnetic nanocomposites with intergranular interaction

S.N. Nikolaev, A.B. Drovosekov, M.Yu. Dmitrieva, K.Yu. Chernoglazov, A.V. Sitnikov, A.N. Taldenkov, A.L. Vasiliev, E.A. Gan'shina, I.M. Pripechenkov, M.A. Simdyanova, A.B. Granovsky, V.V. Rylkov

DOI: https://doi.org/10.3367/UFNe.2024.11.039814

Contents

Abstract. Using the example of nanocomposite (NC) films $(CoFeB)_x(LiNbO_3)_{100-x}$, in which at relatively high temperatures of $T \gtrsim 10$ K a 'weakly insulating' regime is observed in the logarithmic temperature dependence of the conductivity $\sigma \propto \ln T$, characteristic of a strong tunnel coupling between granules, the scaling in the behavior of the anomalous Hall effect (AHE) resistance as a function of the longitudinal resistance ρ was studied in detail. The studies were carried out in fields up to 14 T at temperatures $T = 0.4$–200 K in the range of metallic phase content $x \approx 35-60$ at.%, covering the percolation transition. It was found that the power n in the scaling dependence $\rho_{AHE} \propto [\rho(T)]^n$ behaves nonmonotonically. In the ranges $x \approx 35-44$ at.% and $x \approx 50-60$ at.%, an increase in the power is clearly observed, whereas in the interval $x \approx 44-50$ at.%, the value of n remains practically unchanged. We believe that the kink regions in the dependence $n(x)$ indicate a change in the NC conductivity mechanism and determine the percolation threshold (at $x_p \approx 50$ at.%) and the metal–insulator transition ($x_c \approx 44$ at.%), which do not coincide in these systems. The results of an analysis of the behavior of $\sigma(T)$ at subhelium temperatures $T = 0.4-3$ K confirm this conclusion. Studies of the magnetic properties of NCs vs the metallic phase content x using ferromagnetic resonance and magneto-optical spectroscopy methods also indicate the presence of specific features in the vicinity of concentrations $x \approx 44$ and 50 at.%.

Keywords: anomalous Hall effect, nanocomposites, metal–insulator transition, percolation threshold

S.N. Nikolaev [1,*], **A.B. Drovosekov** [2], **M.Yu. Dmitrieva** [2,3], **K.Yu. Chernoglazov** [1], **A.V. Sitnikov** [1,4], **A.N. Taldenkov** [1], **A.L. Vasiliev** [1,5], **E.A. Gan'shina** [6], **I.M. Pripechenkov** [6], **M.A. Simdyanova** [6], **A.B. Granovsky** [6,7], **V.V. Rylkov** [1,7,8,**]
[1] National Research Center Kurchatov Institute, pl. Akademika Kurchatova 1, 123182 Moscow, Russian Federation
[2] Kapitza Institute for Physical Problems, Russian Academy of Sciences, ul. Kosygina 2, 119334 Moscow, Russian Federation
[3] National Research University Higher School of Economics, ul. Myasnitskaya 20, 101000 Moscow, Russian Federation
[4] Voronezh State Technical University, Moskovskii prosp. 14, 394026 Voronezh, Russian Federation
[5] Moscow Institute of Physics and Technology (National Research University), Institutskii per. 9, 141701 Dolgoprudny, Moscow region, Russian Federation
[6] Lomonosov Moscow State University, Faculty of Physics, Leninskie gory 1, str. 2, 119991 Moscow, Russian Federation
[7] Institute of Theoretical and Applied Electrodynamics, Russian Academy of Sciences, ul. Izhorskaya 13/19, 125412 Moscow, Russian Federation
[8] Kotelnikov Institute of Radioengineering and Electronics, Russian Academy of Sciences, pr. Vvedenskogo 1, 141190 Fryazino, Moscow region, Russian Federation
E-mail: [*] niklser@list.ru, [**] vvrylkov@mail.ru

Received 14 August 2024
Uspekhi Fizicheskikh Nauk **195** (6) 658 – 668 (2025)
Translated by V.L. Derbov

1. Introduction

Granulated metal–dielectric M_xD_{100-x} nanocomposites (NCs) are arrays of granules of ordinary or ferromagnetic (FM) metal, randomly distributed in dielectric matrices [1, 2]. Small granule sizes (2–10 nm) determine specific transport properties of NCs, in particular, the nature of the metal–insulator transition (MIT) that occurs in these systems with a decrease in the metal content x, the understanding of which in granular materials is a complex and not fully resolved theoretical problem [1]. In other words, there is still no

theoretically substantiated criterion for finding the critical point x_c for the MIT in an NC, upon approaching which from above the conductivity of the system σ tends to a finite residual value σ_r at a temperature $T \to 0$, and below this point, $\sigma \to 0$ [1, 3]. On the other hand, in granular NC systems, there is a geometric (or classical) percolation threshold (PT), described in detail by the percolation theory, corresponding to the metal content x_p, at which an infinite cluster of contacting metal granules is formed in the NC, determining the current through the sample. As a result, if the volume fraction occupied by the granules is higher than x_p, then such a composite has metallic conductivity and is often called a 'dirty' metal. Below the PT, the metal granules in the NC are separated by dielectric layers, and therefore the hopping/tunneling mechanism of conductivity is dominant at room temperature and above. Under these conditions, in the immediate vicinity of the PT at $x < x_p$, the so-called weakly insulating (noninterference type) logarithmic mode in the conductivity $\sigma \propto \ln T$ can manifest itself, which, as x decreases, is replaced with the '1/2' law, $\ln \sigma \propto -(T_0/T)^{1/2}$, characteristic of co-tunneling of many electrons through chains of 'resonant' granules [1, 4–9]. In other words, granular systems are very attractive as model objects for studying the interrelated effects of disorder and percolation, electron correlations, Coulomb interaction, and quantum phenomena controlled by the metal content in the NC.

In addition to academic interest in NC systems, there is also increased applied interest, especially in magnetic systems, where many practically important effects are observed: giant magnetoresistance (MR) [10], the anomalous Hall effect with a giant coefficient [11–13], the magnetorefractive effect [14], the enhanced magneto-optical Kerr effect [15], etc. Note also the prospects for their use in radio-absorbing coatings due to their simultaneously high resistance and magnetic softness at certain compositions near the PT [2].

The uniqueness of magnetic NCs is due to the fact that, depending on the matrix material, size, and shape of the granules and their exchange interaction, temperature, and metal concentration, they can be in a single-domain, superparamagnetic, or superferromagnetic state [2, 16–18]. In most earlier studies, it was believed that in these systems there is one critical concentration — the geometric PT x_p, which determines both the metal–insulator transition with a change in concentration and the transition from ferromagnetic (FM) ordering to superparamagnetic (SP) or superferromagnetic (SFM) behavior. However, the possibility of tunneling and exchange interaction between the granules, which can be significantly enhanced, e.g., at a high permittivity of the matrix due to a decrease in the Coulomb interaction and/or the presence of metal ions in it [16–19], leads to the fact that the critical MIT concentration x_c and the concentration of the long-range magnetic order destruction x_f can differ significantly from x_p [2]. In this case, a problem arises with the experimental determination of the important parameters mentioned above and identifying the effect of matrix permittivity, as well as of dispersed metal ions, on the NC properties near the MIT and PT. The concentration dependences of the NC resistance (considering or not considering the values of the critical indices of the percolation theory) under conditions of strong intergranular exchange do not contain sharp irregularities at x_p (see below). Therefore, searching for effective approaches to the experimental determination of critical concentrations (x_c, x_p) and the concentration x_f at which long-range ferromagnetic order is formed in magnetic granular systems turns out to be relevant, in particular by studying the concentration behavior of the anomalous Hall effect (AHE), ferromagnetic resonance (FMR), and the magneto-optical Kerr effect (MOK).

In our recent studies of magnetic NCs $(Co_{40}Fe_{40}B_{20})_x(Al_2O_3)_{100-x}$ and $(Co_{40}Fe_{40}B_{20})_x(LiNbO_3)_{100-x}$ (for brevity, the $Co_{40}Fe_{40}B_{20}$ alloy will be designated as CoFeB), manifestations of superferromagnetic ordering effects, the tunnel AHE, and, in the region of relatively high temperatures, a logarithmic law in the temperature dependence of conductivity that is not associated with weak localization corrections were discovered [9, 20–23]. Recently, nonmonotonic behavior of magnetoresistance with a minimum at 40 K was also discovered [23], which is explained by the coexistence of clusters of superparamagnetic granules and SFM regions with enhanced intergranular exchange, presumably due to the high static permittivity ε_d of the NC matrix [17, 18, 23] (for amorphous $LiNbO_3$ in the frequency range $1-10^3$ kHz $\varepsilon_d \sim 50-90$ [24]). In Ref. [23], based on the data of coercive force studies, it was shown that the temperature of magnetic ordering in the SFM regions reaches $T_{SFM} \approx 230$ K. Note that studies of the magnetic resonance spectra of film NCs $(CoFeB)_x(LiNbO_3)_{100-x}$ demonstrate a change in the mechanisms of magnetic relaxation in the vicinity of the MIT and also exhibit features caused by the presence of exchange interaction between magnetic ions and FM granules [25, 26]. In addition, our detailed studies of MO spectra made it possible to reveal noticeable differences in the magneto-optical spectra in the superparamagnetic, superferromagnetic, and ferromagnetic states of NCs [27].

However, studies [9, 20–23, 25–27] were carried out mainly in the dielectric region of NC compositions below the percolation transition, which initiated this work, namely, comprehensive studies of the behavior of the AHE, FMR, and MOK, starting from the metal side of the PT, with the aim of identifying the critical concentrations x_c and x_p, which determine the metal–insulator transition and the percolation threshold, respectively.

2. Samples and research methods

Films of $(CoFeB)_x(LiNbO_3)_{100-x}$ with a thickness of 100 nm were obtained by ion-beam sputtering on Si substrates using a composite target of a $Co_{40}Fe_{40}B_{20}$ wafer with unevenly distributed $LiNbO_3$ samples, which made it possible to form NCs with different metal contents in the range $x = 35-60$ at.% in a single cycle (see details in Refs [19, 21]). The transport and magnetic properties of NCs were studied in universal samples fabricated by lift-off photolithography in the form of a double Hall cross (width of the conducting channel $w = 1.2$ mm and distance between potential probes on the side faces $l = 1.4$ mm [21]). The experiments were carried out using the multifunctional measuring system PPMS Dynacool-14 in weak electric fields $\leqslant 10$ V sm^{-1}, in the temperature range $T = 3-200$ K, in a magnetic field of up to 14 T. Studies at temperatures of 0.4–30 K were carried out using the ^{3}He insert of the PPMS system.

The microstructure of NC with a nanometer resolution was studied at an accelerating voltage of 200 keV using the transmission/scanning electron microscope (TEM/STEM) Tecnai Osiris (Thermo Fisher Scientific, USA), equipped with a high-angle ring dark-field (HARDF) detector

(Fischione, USA). Studies of the atomic composition by the method of energy-dispersive X-ray (EDX) microanalysis were carried out using a Super-X spectrometer (Bruker, USA), also incorporated in the microscope.

Magnetic resonance studies were performed at room temperature using a laboratory transmission-type spectrometer based on a cylindrical resonator [25]. Absorption spectra were recorded at a constant frequency of $f = 20.6$ GHz with an external magnetic field swept in the plane of the film in the range $H = 0-10$ kOe.

The magneto-optical properties of NCs were studied in the geometry of the equatorial Kerr effect, also called the transverse Kerr effect (TKE), at room temperature in the spectral range of 0.5–4.0 eV in a magnetic field of up to 3.0 kOe. *p*-polarized light was used at an incidence angle of 69.5°. For each concentration, the spectral dependence in the maximum magnetic field and the temperature and field dependences of the TKE signal for selected wavelengths were measured. The measurements were performed using a dynamic method, in which the TKE parameter is the relative change in the intensity of reflected light when the sample is magnetized by an alternating magnetic field with a frequency of 40 Hz.

3. Results and discussion

3.1 Structural features of samples

A low-magnification bright-field STEM image of the cross-section of the $(CoFeB)_x(LiNbO_3)_{100-x}$/Si structure is shown in Fig. 1a. This image shows the nanocomposite layer (dark contrast), the Si substrate, and the transition amorphous SiO_x layer with a thickness of ≈ 10 nm, formed in the course of the NC film deposition. The uniform contrast in the low-magnification image indicates the uniformity of the composition of the NC film, the thickness of which is 100 ± 2 nm. The high-resolution TEM (HRTEM) image is shown in Fig. 1b. The mass-thickness contrast clearly indicates the presence of relatively dense granules with average lateral size $a_g \approx 2.5$–2.7 nm, slightly elongated in the NC growth direction (by no more than 1.5 times). Elemental EDX mapping clearly showed that the granules mainly contain Fe and Co. Note that, in the previously studied NC $(CoFeB)_x(LiNbO_3)_{100-x}$ films grown on sitall (glass ceramics), we observed by HRTEM methods the crystallinity of individual granules in the bcc structure with the unit cell constant $a_c = 0.284$ nm, characteristic of the intermetallic compound CoFe [21]. In the NC films of $(CoFeB)_x(LiNbO_3)_{100-x}$ grown on silicon, a detailed analysis of HRTEM images with the recording of two-dimensional Fourier spectra did not reveal periodicity (see the inset in Fig. 1b and compare with similar spectra in Fig. 2 from Ref. [21]). This circumstance indicates a significantly higher content of boron atoms in the Co-Fe-B granules, which promotes their amorphization [28], and probably a decrease in the density of electron states at the Fermi level in the granules. The latter, according to Ref. [5], facilitates the temperature transition to elastic co-tunneling, leading in our case at $T \leqslant 20$ K to a strong increase in the negative MR with decreasing temperature [23], which in relatively weak fields can be associated with co-tunneling spin-dependent processes [29], and in strong fields, most likely, is due to quantum interference effects [5].

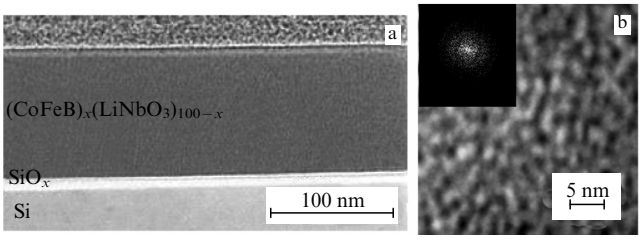

Figure 1. (a) Bright-field STEM image of $(CoFeB)_x(LiNbO_3)_{100-x}$ nanocomposite film with $x \approx 40$ at.%. (b) High-resolution transmission electron microscopy (HRTEM) image of NC film in dark-field mode. Bright contrast corresponds to granules with a size of $a_g \approx 2.5-4$ nm. Inset shows typical two-dimensional Fourier spectrum from CoFeB granule.

We also note that, under the conditions considered, a lower boron content is expected in the $LiNbO_{3-y}$ matrix and, consequently, its higher effective permittivity, since boron in the matrix is mainly in the form of oxide [30], possessing a relatively low permittivity (for B_2O_3, the value is $\varepsilon_d \sim 4$ [31]). (A quantitative analysis of the part of boron that finds itself in the oxide matrix during NC growth is not possible using the existing EDX methods [9, 21].)

3.2 Conductivity

The key role in describing the transport properties of granular metals below the PT ($x < x_p$) is played by the concept of the average tunnel conductance between neighboring granules G_t [1, 4]. According to Refs [1, 4], for small intergranular gaps, when the value of G_t significantly exceeds the conductivity quantum, i.e., $g = G_t/(2e^2/\hbar) \geqslant 1$, the conductivity of NCs with ordered arrangement of granules follows the law

$$\sigma(T) = \sigma_0\left(1 - \frac{1}{\pi k g}\ln\left[\frac{gE_C}{k_B T}\right]\right) \propto \beta \ln T, \qquad (1)$$

where k is the coordination number of the periodic lattice (the number of contacts of a granule with its nearest neighbors), k_B is the Boltzmann constant, and $E_C = e^2/(\varepsilon_d a_g)$ is the Coulomb blockade energy. The logarithmic conductivity law (1) is explained by the renormalization of the Coulomb interaction rather than being related to corrections due to weak localization [1, 4]. Therefore, to observe it, the temperature should not be too low or too high: $g\delta \ll k_B T \ll E_C$, where δ is the average separation between the energy levels in an individual granule.

When the content of metal granules is below a certain value x_c, the dimensionless conductance g is less than the critical value $g_c \lesssim 1$. Under these conditions, according to Ref. [1], a metal–insulator transition occurs, below which a 'strongly insulating' law in conductivity should be observed — the Efros–Shklovsky '1/2': $\ln\sigma \propto -(T_0/T)^{1/2}$, caused by co-tunneling of electrons through chains of 'resonant' granules (T_0 being a parameter that increases with increasing E_C and decreasing the electron localization length on the granules). Strictly speaking, the metal content for the transition to the strongly insulating activation mode of conductivity x_{sc} may differ from x_c for the MIT ($x_{sc} \leqslant x_c$) [1, 7].

On the other hand, at $x > x_p$, the role of the Coulomb blockade is suppressed and one should expect a shift of the logarithmic law to the region of helium temperatures, where it should be determined by weak localization corrections, as in dirty metal thin films [3, 4].

In NCs based on a pure metal and a wide-gap dielectric with a low value of ε_d (e.g., like Ni-SiO_2 [7]), the percolation

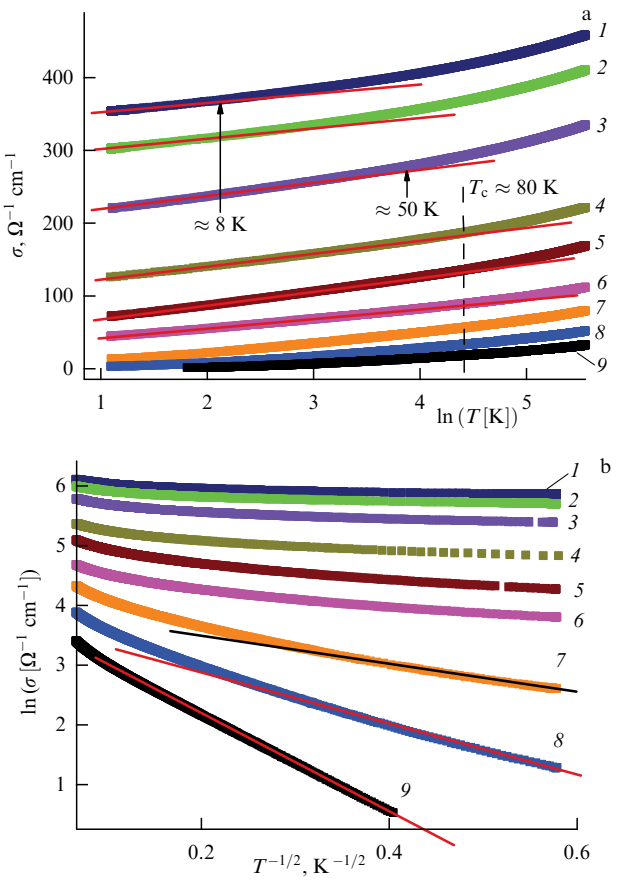

Figure 2. Temperature dependences of conductivity $\sigma(T)$ of $(CoFeB)_x(LiNbO_3)_{100-x}$ films in coordinates $\sigma - \ln T$ (a) and in coordinates $\ln\sigma - (1/T)^{1/2}$ (b). Dependences were obtained for samples with different contents of ferromagnetic alloy (in at.%): curve *1* — 57; *2* — 54; *3* — 52; *4* — 50; *5* — 46; *6* — 44; *7* — 43; *8* — 41; *9* — 38.

transition is usually easily detected by a change of sign of the temperature coefficient of resistance $\alpha = d\rho/dT$ (where $\rho = 1/\sigma$); at $x > x_p$ the coefficient $\alpha > 0$, whereas below the PT, the sign of α turns out to be negative ($\alpha < 0$) [7]. However, this method cannot always be justified in NCs based on highly resistive metallic materials, in which even in a homogeneous case, according to the Mooij rule, the coefficient α can be negative [32]. Particularly, in our case, the amorphous metallic alloy $Co_{40}Fe_{40}B_{20}$ itself has $\alpha < 0$ (Fig. 6 from Ref. [33]). Therefore, the sign of α obviously does not change when passing through the PT and a different approach to the analysis of the x_p value is necessary.

The temperature dependences of the conductivity $\sigma(T)$ in the studied structures are shown in Fig. 2. For an NC with a metal content of $x \approx 46-50$ at.%, the conductivity in a relatively wide temperature range (even to highs of $T_c \approx 80$ K) is described by the logarithmic law $\sigma \propto \ln T$ (Fig. 2a), characteristic of a strong tunnel coupling between neighboring granules [4] (a 'weakly insulating' tunnel conductivity mode). With a further decrease in x, in accordance with [1, 4], a transition to a 'strongly insulating' mode occurs, where an exponential '1/2' law is observed in $\sigma(T)$, which in our case is clearly manifested in samples with $x \leqslant x_{sc} \approx 43$ at.% (Fig. 2b). Previously, a similar behavior of $\sigma(T)$ was observed by us in NC films of $(CoFeB)_x(Al_2O_3)_{100-x}$ with a change in x from 56 to 47 at.% ($x_p \approx 57$ at.%) [9]. However, in Ref. [9], the logarithmic law $\sigma \propto \ln T$ was observed up to room temperature, while in the case under consideration this law holds only up to $T_c \approx 80$ K. The explanation is that the applicability of the theory [4], as noted above, is limited by the condition $k_B T \ll E_C = e^2/(\varepsilon_d a_g)$. Assuming $T_c \approx E_C/k_B = e^2/(a_g k_B \varepsilon_d)$ and taking into account that the permittivity of Al_2O_3 $\varepsilon_d \approx 10$, we find for the amorphous matrix $LiNbO_{3-y}$ the effective value $\varepsilon_d \approx 10 \times 300/80 \approx 40$, which correlates well with the available data for a-$LiNbO_3$ [24].

On the other hand, when the content of the metallic phase is above 50 at.%, a significant shift to the low-temperature region occurs in the upper limit of the observation of the logarithmic law $\sigma \propto \ln T$, namely, up to $T_c \approx 50$ K at $x \approx 52$ at.% and $T_c \approx 8$ K at $x \approx 57$ at.% (Fig. 2a). This indicates that for $(CoFeB)_x(LiNbO_3)_{100-x}$ films the percolation threshold x_p is about 50 at.%, above which, according to [1, 4], a transition to the dirty metal conductivity mode occurs.

Thus, the above analysis of the temperature dependences of the $(CoFeB)_x(LiNbO_3)_{100-x}$ NC system shows the presence of the following conductivity modes as the composition changes. At $x \leqslant x_{sc} \approx 43$ at.%, the 'strongly insulating' mode takes place with an exponential conductivity dependence, $\sigma(T) \propto \exp[-(T_0/T)^{1/2}]$. As x increases, this mode is first replaced by a 'weakly insulating' tunnel mode with the logarithmic law of conductivity, $\sigma \propto \ln T$, and then above the PT threshold ($x > x_p \approx 50$ at.%), by a diffusion conductivity mode of a 'dirty' metal [1].

Additionally, to prove the existence of an MIT and the presence of a 'weakly insulating' metallic state [1, 3] in the studied system, we carried out studies of low-temperature conductivity (0.4–30 K) using a ^{3}He insert to the PPMS measuring system (Fig. 3). Analysis of the dependences of the normalized conductance $G(T)/G(10\text{ K})$ on $\ln T$ shows that, at $x < x_p \approx 50$ at.%, the most significant deviations from the logarithmic law occur below 3 K (see Fig. 3a and the inset in it). To analyze the dependences $G(T)$ under such conditions, we used the description of the transport properties of disordered systems near the MIT, based on the scaling hypothesis, which has been tested well enough by the example of doped semiconductors [3], especially since there is a certain analogy between the conductivity of granular metals and doped uncompensated semiconductors [34]. Based on this hypothesis, in the immediate vicinity of the MIT, in the 3D case $\sigma(T) = \alpha + \beta T^{1/3}$, and exactly at the transition, $\alpha = 0$. Therefore, to find the transition point, it is necessary to plot the dependences of σ on $T^{1/3}$ for various MIT control parameters (for NC, the control parameter is the metal content x) and find one at which $\alpha \approx 0$ at $T^{1/3} \to 0$. In our case, the dependences of the normalized conductance are well straightened in the coordinates $G/G(10\text{ K}) - T^{1/3}$, and the ratio $G/G(10\text{ K})$ turns out to be finite and positive at $x \approx 44$ at.% ($G/G(10\text{ K}) \approx 0.1$, $\sigma(0) \approx 10\ \Omega^{-1}\text{ cm}^{-1}$) and obviously negative at $x \approx 43$ at.% (Fig. 3b). Therefore, the sample with $x \approx 44$ at.% is 'metallic,' whereas the sample with $x \approx x_{sc} \approx 43$ at.% is a dielectric with hopping conductivity activation. In this case, the MIT point x_c is obviously shifted to the region of higher contents in comparison with x_{sc} by a value less than 1 at.%, i.e., less than the absolute error in measuring the NC composition (about 1 at.%). It is interesting to note that in our case the magnetic field enhances electron localization (see the inset in Fig. 3b), just as in doped semiconductors [3, 35]. At $B = 10$ T, the residual conductivity $\sigma(0) > 0$ is positive and amounts to $\approx 3\ \Omega^{-1}\text{ cm}^{-1}$, i.e., the sample still remains on the metal side

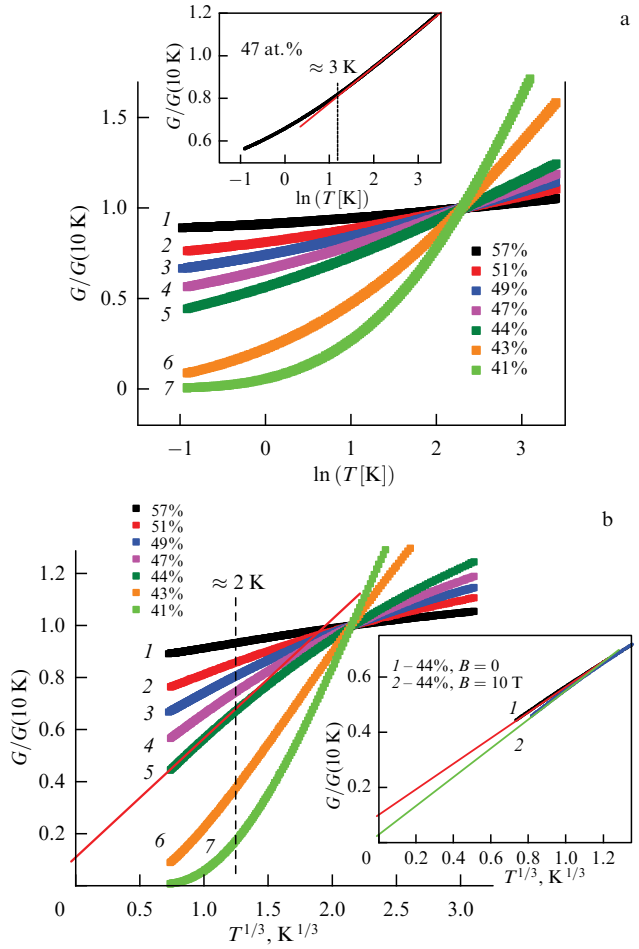

Figure 3. Temperature dependences of conductance $G(T)$ of $(CoFeB)_x(LiNbO_3)_{100-x}$ films, normalized to value of G at 10 K in $G-\ln T$ coordinates (a) and in $G-T^{1/3}$ coordinates (b). Curves *1*–*7* were obtained for samples with different contents of ferromagnetic alloy (alloy content in at.% and conductivity at 10 K in Ω^{-1} cm^{-1} are indicated after curve number): curve *1* — 57.372; *2* — 51.180; *3* — 49.162; *4* — 47.148; *5* — 44.101; *6* — 43.26; *7* — 41.11. Upper inset shows dependence of G on $\ln T$ on an enlarged scale for sample with $x \approx 47$ at.%. Lower inset shows dependence of G on $T^{1/3}$ for sample with $x = 44$ at.% in field of $B = 0$ and 10 T.

of the MIT. The mechanism of the influence of the magnetic field on the localization of electrons and the MIT in magnetic NCs seems, in our opinion, different (see, e.g., [36]) than in semiconductors (compression of the wave functions of electrons localized on impurities) and requires separate studies.

Let us further consider the features of AHE behavior in the presence of a region with a 'weakly insulating' tunnel conductivity regime.

3.3 Anomalous Hall effect

In the general case, the AHE in ferromagnetic materials is determined by the spin-orbit interaction (SOI) and the spin polarization of charge carriers, proportional to the magnetization M of the sample [37]:

$$\rho_H = R_0 B + 4\pi R_s M \approx 4\pi R_s M\,, \qquad (2)$$

where ρ_H is the specific Hall resistance. The first term in Eqn (2) describes the normal Hall effect, proportional to the magnetic induction B and caused by the Lorentz force; R_0 is the constant of the normal Hall effect, M is the magnetization. The second term is determined by the anomalous component of the Hall effect $\rho_{AHE} = 4\pi R_s M$, which, in ferromagnetic materials, including magnetic granular systems [7, 11, 12], is usually dominant, $\rho_{AHE} \gg R_0 B$. In many cases, the AHE constant R_s depends on the longitudinal resistivity ρ according to a power law, $R_s \propto \rho^n$, where the exponent n is determined by the AHE mechanism. At low temperatures, when $M(T) \approx$ const, $\rho_H \approx \rho_{AHE} = 4\pi R_s M \propto R_s$, i.e., $\rho_H \propto \rho^n$. Scaling is also often expressed in terms of the Hall conductivity, $\sigma_H = \rho_H \sigma^2$, in this case, $\sigma_H \propto \sigma^\gamma (\gamma = 2 - n)$.

In theory, the relationship between the exponent n and the AHE mechanism is well established for homogeneous ferromagnets with metallic conductivity upon elastic scattering of charge carriers (low temperatures). In this case, $n = 1$ for the skew scattering and $n = 2$ for the side-jump mechanism during scattering and the intrinsic AHE mechanism [37]. It has also been established experimentally and theoretically that in 'dirty' metallic systems with strong impurity scattering at a resistivity of $\rho > 10^{-4}$ Ω cm, the value of n decreases to $n \approx 0.4$ [37–40]. Note that, in experiments studying scaling (determining n), as a rule, the conductivity of samples is varied by changing the content of defects (scattering centers) at a fixed temperature [37–39].

The situation is different in granular systems. In this case, above the PT in its immediate vicinity ($x \geqslant x_p$), the value of $n = 0.6-0.7$ [7, 11], falling to $x \lesssim x_p$ at $n \approx 0.24$ [9, 22], was obtained from the experiment. It seems natural to use the Efetov AHE model [41] to explain this behavior. In this model, the AHE of a granular system in the 'weakly insulating' tunnel mode ($x_{sc} < x < x_p$) was considered and it was shown that, in this case, $n \approx 0$. This is explained by the fact that, for the granule conductance $G_g \gg G_t$, the resistance of the system as a whole is determined by the intergranular gaps, whereas the AHE is formed inside the granules [41]. Note that, in Ref. [41], the AHE in granules was considered within the framework of the skew scattering and side-jump models, and the possibility of the occurrence of tunnel AHE (TAHE) at the interfaces of granules and in the gaps between them [42–44] (see also [45] and references therein) was not taken into account, nor was the AHE associated with a correlated change in the probability of co-tunnel transitions in a set of three or more centers (granules) under the effect of the SOI [22, 46, 47]. Apparently, such a situation is realized in NC based on Ni-SiO_2-type stoichiometric wide-bandgap dielectrics with high and relatively narrow barriers between the granules [7]. In Ref. [7], in accordance with the prediction of [41], a flattening in the parametric dependence of $\log_{AHE}$ on $\log \rho(x) (n \approx 0)$ was found for resistivity values from the region of the 'weakly insulating' tunnel conductivity regime (10^{-2} Ω cm $< \rho < 1$ Ω cm). Above the PT ($\rho < 10^{-2}$ Ω cm), a power law $\rho_{AHE} \propto \rho^n$ with $n \approx 0.6-0.7$ was observed [7]. In other words, in this case, observing a 'break' in the dependence of $\log \rho_{AHE}$ on $\log \rho(x)$ allows us to determine the value of x_p (Fig. 1a from Ref. [7]).

However, as we have established [9, 22], in NCs based on nonstoichiometric oxides such as Al_2O_{3-y} and $LiNbO_{3-y}$, the TAHE is noticeably manifested in the 'weakly insulating' tunnel mode. It will be shown below that, in this situation, the analysis of the parametric dependence of $\log \rho_{AHE}$ on $\log \rho(x)$ no longer allows extracting information about the values of x_p and x_{sc}, and additional analysis of the temperature

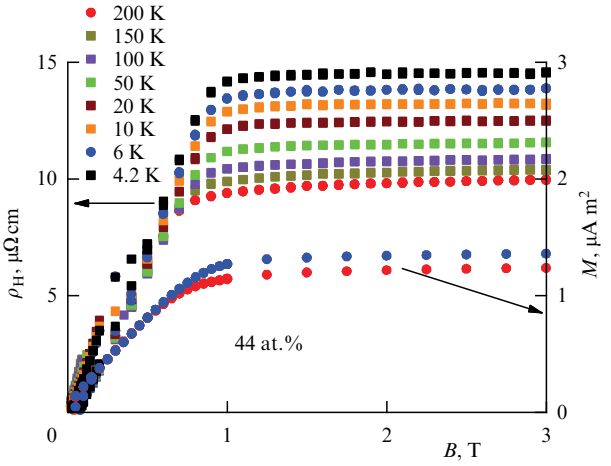

Figure 4. Magnetic field dependences of Hall resistance ρ_H and magnetization M for sample of $(CoFeB)_x(LiNbO_3)_{100-x}$ with content $x = 44$ at.% at different temperatures.

behavior of the AHE scaling in samples with different content x is necessary.

Typical magnetic field dependences of the Hall resistivity ρ_H and magnetization M for a sample with $x = 44$ at.% at different temperatures are shown in Fig. 4. From the data in Fig. 4, it follows that in the studied NCs the behavior of the AHE correlates well with that of the magnetization, which, like the AHE, is saturated in a field $B_s \approx 1$ T. The virtual absence of slope in ρ_H under the conditions of magnetization saturation indicates the dominance of the AHE and small value of the normal component of the Hall effect, i.e., in our case, $\rho_H \approx \rho_{AHE}$. With a decrease in temperature from 200 to 6 K, the magnitude of the AHE increases by almost 1.5 times, while the magnetization changes by no more than 8%. Therefore, in fields above > 1 T, it can roughly be assumed that $\rho_{AHE} \propto R_s \propto \rho^n$ (in the same form that scaling was studied in Refs [7, 11]). We also note that, according to the magnetization measurement data in the $(CoFeB)_x(LiNbO_3)_{100-x}$ NCs under study, $N_d \sim 4 \times 10^{20}$ cm^{-3}, as in [22], i.e., the minimum is an order of magnitude smaller than in the previously studied $(CoFeB)_x(Al_2O_3)_{100-x}$ samples [9].

Let us now turn to the scaling behavior of the Hall resistance of the synthesized NC samples, which, as noted above, is usually studied at a fixed temperature to avoid the influence of inelastic scattering of electrons by phonons and/or magnons, which can lead to rather strong changes in the exponent of the dependence $\rho_{AHE} \propto \rho^n$ when temperature is used as a variable parameter [9, 48, 49].

Figure 5a shows the parametric dependence of the $\rho_{AHE}[\rho(x)]$ on a double logarithmic scale, i.e., in the same form as in Ref. [7]. It is evident that, in the range of longitudinal resistance ρ from 7×10^{-3} to 2×10^{-1} Ω cm, the experimental points, within the graphic accuracy, lie on a straight line with a nonzero slope of $n \approx 0.29$, which we associate with the manifestation of the TAHE [9, 22]. At the same time, there are no indications of a PT similar to those found in Ref. [7]. In Refs [9, 22], we normalized the AHE resistivity ρ_{AHE} by the value of x to compensate for the effect of changing the magnetization of the samples on the scaling behavior of the AHE coefficient. The dependence of $\ln(\rho_{AHE}/x)$ on $\ln[\rho(x)]$ for the samples under study is shown in Fig. 5b. In this case, the scatter of points decreases

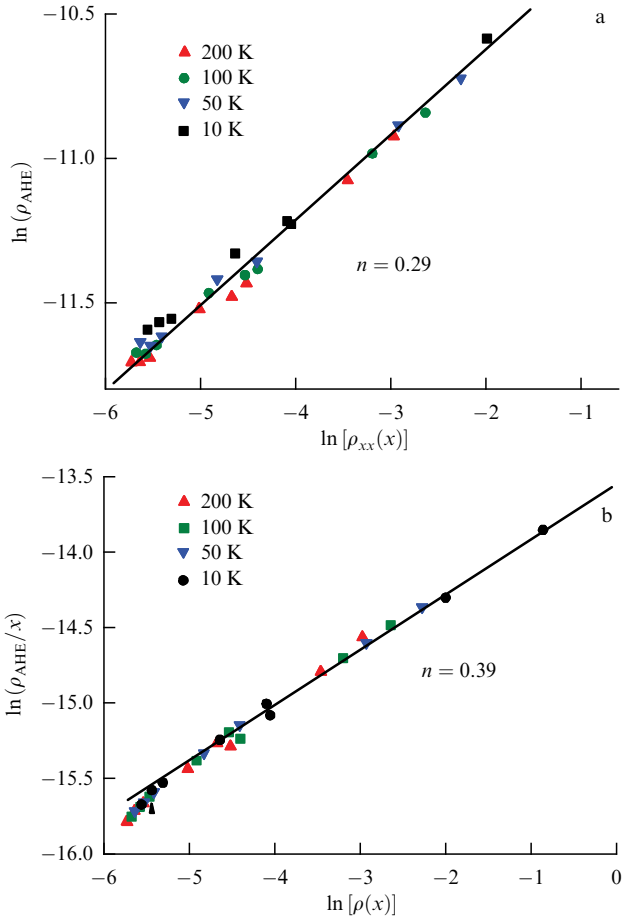

Figure 5. (a) Dependence of Hall resistance on longitudinal resistance at fixed temperature and varying composition. (b) Dependence of Hall resistance normalized to metal content on longitudinal resistance at fixed temperature and varying composition.

and, at $x \geqslant 55$ at.%, a clear deviation from the linear law is observed in this dependence, which can be associated with the manifestation of the PT.

In our recent paper [22], the parametric dependences of $\ln \rho_{AHE}$ on $\ln[\rho(T)]$ were studied in detail below the PT, and it was shown that their slope (the exponent n) changes noticeably (by a factor of ~ 1.5) when the conductivity '1/2' law, $\ln \sigma \propto -(T_0/T)^{1/2}$, changes to the logarithmic law, $\sigma \propto \ln T$. This tendency is also preserved in the samples studied when x changes in a wider range: the value of n increases 0.32 from $x \approx 40$ at.% to $n \approx 0.67$ at $x \approx 58$ at.% (Fig. 6). In this connection, a natural idea arises about a detailed study of the concentration dependence of the exponent $n(x)$, found by varying the temperature, with the aim of identifying singular points that may arise when the conductivity mechanism changes, being reflected by a change in the temperature dependence $\sigma(T)$ (see Section 3.2).

The obtained dependence $n(x)$ for samples with a metal content of $x \approx 35-60$ at.% is shown in Fig. 7a. As follows from the data presented in the figure, the exponent n in the scaling dependence $\rho_{AHE} \propto [\rho(T)]^n$ behaves nonmonotonically as the content of the metallic phase changes. In the range of $x \approx 35-44$ at.%, corresponding to the conductivity law $\ln \sigma \propto -(T_0/T)^{1/2}$, the exponent increases 1.5 times from $n \approx 0.31$ to $n \approx 0.45$. Meanwhile, with a content of $x \approx 44-50$ at.%, the value of n remains practically

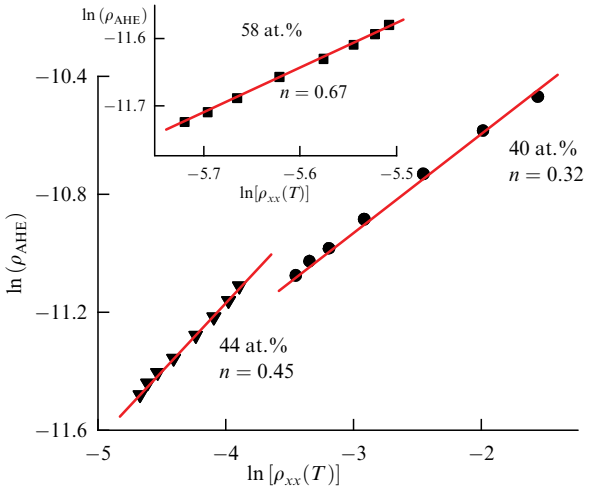

Figure 6. Dependences of Hall resistance on longitudinal resistance for samples of $(CoFeB)_x(LiNbO_3)_{100-x}$ with metal content of 40, 44, and 58 at.%, obtained by varying temperature.

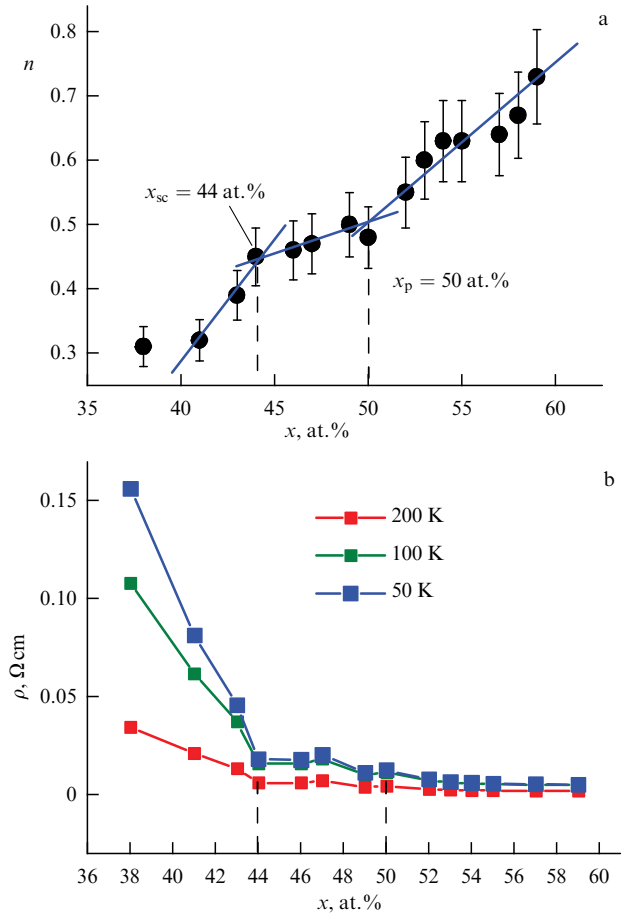

Figure 7. (a) Dependence of exponent n of scaling $\rho_{AHE} \propto [\rho(T)]^n$ on content of metal component in samples of $(CoFeB)_x(LiNbO_3)_{100-x}$. (b) Dependences of resistivity of NC films of $(CoFeB)_x(LiNbO_3)_{100-x}$ on content of metal phase at temperatures of 50, 100, and 200 K.

unchanged, $n \approx 0.45-0.48$. Recall that in this range the conductivity obeys the logarithmic law $\sigma \propto \ln T$ up to 80 K. With a further increase in the metal content, $x \approx 50-60$ at.%, a clear increase in the exponent is observed, $n \approx 0.48-0.7$. In the theoretical paper [47], considering impurity magnetic semiconductors, in the hopping conductivity mode, the values of $n = 0.38-0.67$ were obtained, coinciding with our experimental data for samples in the 'strongly and weakly insulating' tunnel conductivity modes, $n \approx 0.31-0.48$.

For comparison, Fig. 7b shows the dependences of the resistivity of NC films of $(CoFeB)_x(LiNbO_3)_{100-x}$ on the content of the metal phase at different temperatures. It is noteworthy that the kink in the plot of $n(x)$ observed at 44 at.% (Fig. 7a) coincides with the beginning of the region of a sharp increase in ρ with decreasing x (Fig. 7b), associated with the transition at $x_{sc} \approx 43$ at.% to the 'strongly insulating' regime with the co-tunneling conductivity mechanism, $\ln\sigma \propto -(T_0/T)^{1/2}$ [1]. In this system, it practically coincides with the point for the MIT $x_c \approx 43-44$ at.%. At the same time, the transition at $x < 50$ at.% to the 'weakly insulating' tunneling conductivity regime, when $\sigma \propto \ln T$, manifests itself in $\rho(x)$ rather weakly (Fig. 7b).

Thus, the regions of kinks in the dependence $n(x)$ indicate changes in the NC conductivity mechanism and determine the percolation threshold (at $x_p \approx 50$ at.%) and the transition from the weakly insulating to the strongly insulating conductivity regime ($x_{sc} \approx 43$ at.%), which differ noticeably in these systems. In this case, the percolation transition region in the dependence of resistivity $\rho(x)$ does not contain any striking singularities. It turns out that, under such conditions, the exponent determined by the AHE mechanism reflects the transport features of the NC much more strongly when its composition changes than the type of temperature dependence of resistance.

Let us further consider the features of the behavior of magnetic resonance and the magneto-optical Kerr effect in the PT and MIT regions.

3.4 Magnetic resonance

Figure 8 shows the experimental FMR spectra for a series of NC films of $(CoFeB)_x(LiNbO_3)_{100-x}$ with different contents of the FM phase x, measured at room temperature at a frequency of $f = 20.6$ GHz. Note that, with increasing x in the range of $x = 35-60$ at.%, the FMR line intensity monotonically increases, and its width ΔH decreases. In this case, the observed shift of the absorption peak H_{res} to low fields is due to the increase in the effective demagnetization field $4\pi M_{eff}$ of the films according to the well-known Kittel formula for FMR:

$$f = \gamma\left[H_{res}(H_{res} + 4\pi M_{eff})\right]^{1/2}, \qquad (3)$$

where γ is the gyromagnetic ratio corresponding to the effective g-factor for the CoFeB alloy $g_{eff} \approx 2.1$ [25].

Figure 9 shows the resulting experimental dependences of the values of $4\pi M_{eff}(x)$ and $\Delta H(x)$ on concentration x. It can be noted that the dependence of $4\pi M_{eff}(x)$ exhibits a kink in the vicinity of $x \approx 44$ at.% (Fig. 9a), corresponding to the transition to the highly insulating transport mode x_{sc} (or the MIT at $x_c \approx 43-44$ at.%) according to the conductivity measurements. In this case, above x_{sc}, the proportionality of $4\pi M_{eff}(x) \propto x$ is fulfilled, which may indicate a significant increase in intergranular exchange and the formation of an ordered FM film. Below this concentration ($x \lesssim x_{sc}$), the interaction between the granules decreases, and the value of $4\pi M_{eff}(x)$ begins to rapidly decrease due to amplification of thermal fluctuations of FM granules (transition to a superparamagnetic state).

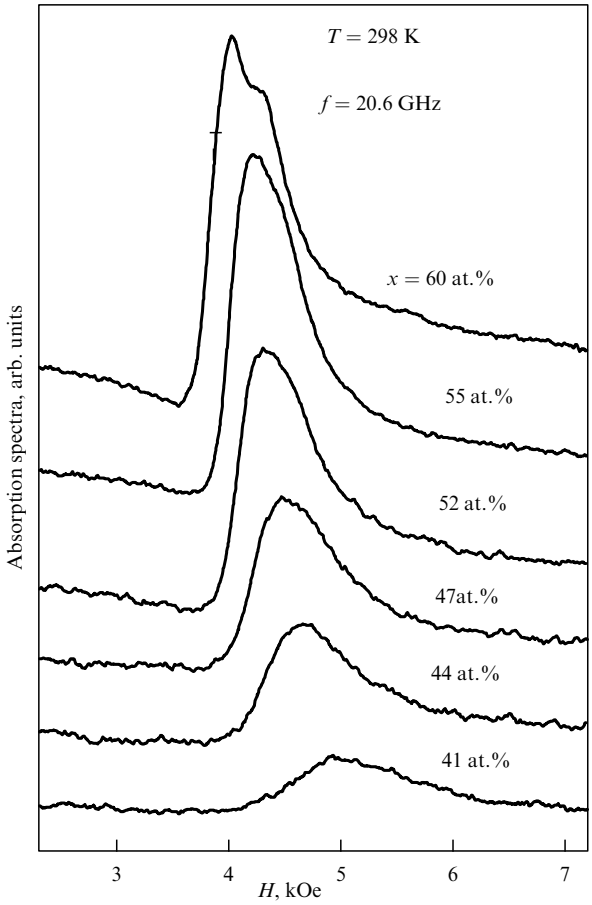

Figure 8. FMR spectra in samples of $(CoFeB)_x(LiNbO_3)_{100-x}$ with various contents of magnetic phase.

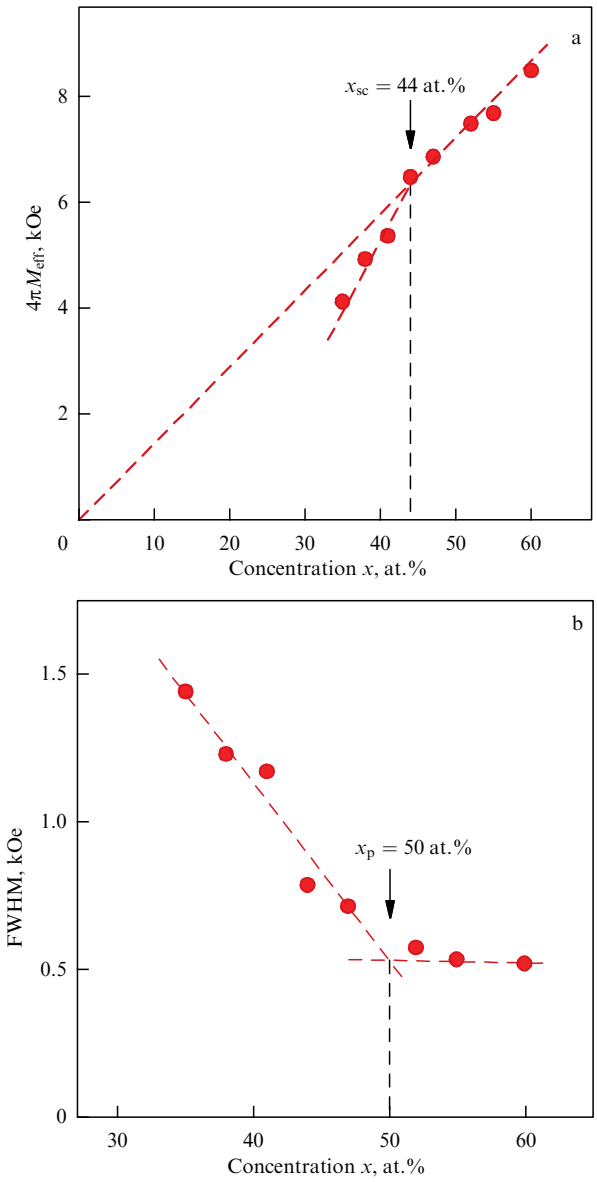

Figure 9. Concentration dependences of value of $4\pi M_{eff}$ (a) and FMR linewidth ΔH (b).

The concentration dependence of the FMR line width $\Delta H(x)$ shows a kink in the vicinity of $x \approx 50$ at.%, close to the PT of films x_p according to the transport measurements (Fig. 9b). Moreover, above this threshold ($x > x_p$), the line width practically reaches the constant value $\Delta H \approx 0.05$ kOe, and below ($x < x_p$), it begins to increase sharply. This behavior can be explained by a significant increase in the inhomogeneous broadening of the FMR line below the PT of films. Note that, according to the data from Ref. [25], the magnetic inhomogeneity of $(CoFeB)_x(LiNbO_3)_{100-x}$ films is the main source of FMR line broadening in the vicinity of the MIT. In this case, in the concentration range $x < x_c \approx 43-44$ at.%, the inhomogeneous broadening of the FMR line is better described in the approximation of weakly interacting independent FM granules. On the contrary, for $x > 44$ at.%, the two-magnon scattering model, which considers the presence of magnetic defects in a quasi-homogeneous FM film, turns out to be more adequate.

3.5 Magneto-optical Kerr effect

In the transverse Kerr effect (TKE) geometry, a relative change in the intensity of the *p*-polarized light reflected from the sample is measured upon magnetization of the sample. Therefore, the TKE parameter depends both on the light frequency, which is the basis of magneto-optical spectroscopy, and on the magnitude of the applied field [50]. For homogeneous ferromagnets, the TKE parameter depends linearly on the magnetization, but this is not true for inhomogeneous ferromagnets, in particular for NCs, since, in this case, separately located superparamagnetic granules and ferromagnetically ordered regions are characterized by fundamentally different field dependences [27, 50]. For the dielectric region of NCs (< 43 at.%), with increasing x, it was possible using field dependences to reveal a transition from the superparamagnetic state to a mixed state, in which superparamagnetic granules coexist with superferromagnetic regions and, ultimately, a transition to a long-range ferromagnetic order [27].

Figure 10 shows the field and spectral dependences of the TKE for samples containing from 43 to 59 at.% of ferromagnetic metal. From the field dependences of the TKE presented in Fig. 10 in an unnormalized form (Fig. 10a) or normalized to the signal in the maximum field (Fig. 10b), it follows that the TKE field dependence at $x = 43$ at.% differs significantly from the one for $x = 47$ at.%, as well as for $x = 55$ and 59 at.%. These characterize soft magnetic samples that are easily magnetized in weak fields (less than 100 Oe), whereas at $x = 43$ at.% the sample is not magnetized to

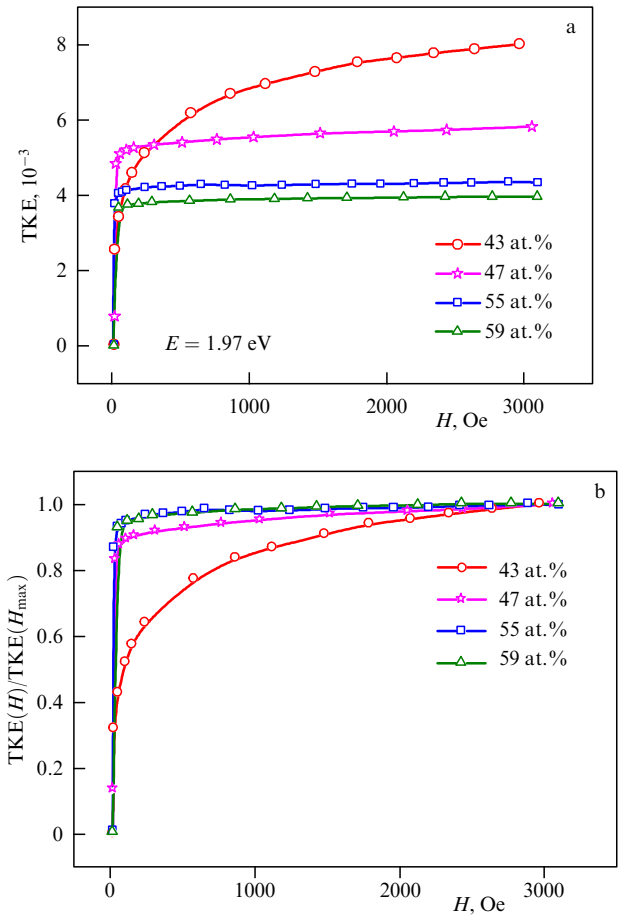

Figure 10. Field dependences of TKE in nanocomposite $(CoFeB)_x(LiNbO_3)_{100-x}$ at $E = 1.97$ eV in nonnormalized form (a) and normalized to maximum-field signal (b).

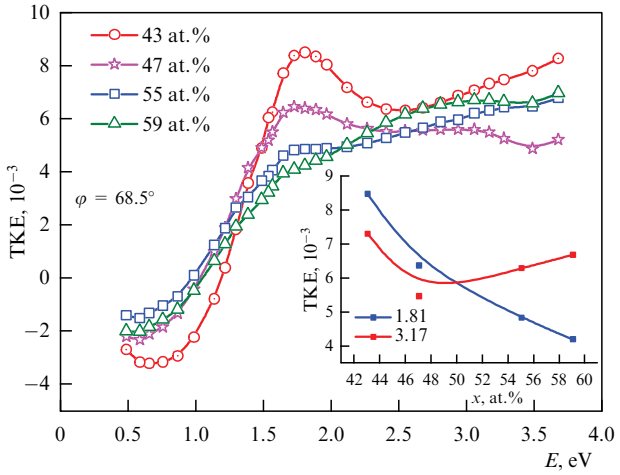

Figure 11. Spectral dependences of TKE in $(CoFeB)_x(LiNbO_3)_{100-x}$ nanocomposite. Inset shows TKE dependences on magnetic phase content at energies of 1.81 and 3.17 eV.

saturation even in a field of 3 kOe. Moreover, it is evident from Fig. 10a that the TKE signal for the sample with $x = 55$ at.% at 1.97 eV is lower than at $x = 43$ or 47 at.%, although it has a higher content of the ferromagnetic component. These data unambiguously testify to the fact that, at $x = 43$ at.%, there are free-standing superparamagnetic granules, and in an overwhelming proportion to possible ferromagnetic or superferromagnetic regions. That is, indeed, the transition to the 'strongly insulating' regime occurs in the vicinity of $x_c = 43-44$ at.%, which is in good agreement with the data from magneto-transport measurements.

In early paper [15] devoted to magneto-optical spectroscopy of NCs, it was suggested that the minimum in the spectral dependence of the TKE in the near-IR region of the spectrum is achieved for nanocomposites at the percolation threshold, but it was not specified whether this concentration is the geometric PT or the corresponding MIT. As can be seen from Fig. 11, the minimum of the TKE in the near-IR region of the spectrum is achieved at 0.7 eV in the vicinity of 43–44 at.%, i.e., in the vicinity of the MIT. Magneto-optical spectra are determined by interband magneto-optical and intraband transitions. Whereas the role of intraband transitions is insignificant in the visible region of the spectrum, as the wavelength increases, intraband transitions become competitive with interband ones. Therefore, when continuous metal paths are destroyed, intraband transitions are suppressed and the spectrum changes, which is the main reason for the different concentration dependences of a TKE signal in saturation at different wavelengths. The inset in Fig. 11 shows examples of the TKE concentration dependences. For the ultraviolet spectrum region, the TKE minimum is observed near $x \approx 48$ at.%, i.e., near the geometric PT. To summarize, we conclude that the field and spectral dependences of the TKE can also be used to identify the PT and MIT.

4. Conclusion

The performed comprehensive study of the electrical resistance, AHE, FMR, and MOK effect in $(CoFeB)_x(LiNbO_3)_{100-x}$ nanocomposites with different contents x of the ferromagnetic phase showed that the geometric percolation threshold does not coincide with the critical concentration of the metal–insulator transition. The concentration dependences of electrical resistance do not allow revealing this difference, whereas a change in the AHE scaling when varying the ferromagnetic phase concentration makes it possible to determine the above critical concentrations as $x_p \approx 50\%$ for the geometric percolation threshold and $x_c \approx 43-44$ at.% for the metal–dielectric transition. The results of analyzing the conductivity behavior of NC films at subhelium temperatures $T = 0.4 - 3$ K made it possible to show that in the studied system the transition to the 'strongly insulating' activation conductivity mode $x_{sc} \approx 43$ at.% is shifted relative to the metal–insulator transition by an amount not exceeding 1 at.%. The high sensitivity of the precision FMR and MOK magnetic methods also made it possible to reveal features in the vicinity of the same compositions, thereby confirming the proposed method for analyzing the AHE scaling, which can be used for any magnetic nanocomposites.

The study was carried out with financial support from the Russian Science Foundation (grant no. 22-19-00171) in terms of studying the transport properties of film NCs and the State Assignment to the National Research Center Kurchatov Institute in terms of studying the features of their microstructure. The equipment of the Resource Center was used in the research.

References

1. Beloborodov I S et al. *Rev. Mod. Phys.* **79** 469 (2007)
2. Bedanta S, Kleemann W *J. Phys. D* **42** 013001 (2009)
3. Gantmakher V F *Electrons and Disorder in Solids* (Oxford: Oxford Univ. Press, 2005); Translated from Russian: *Elektrony v Neuporyadochennykh Sredakh* (Moscow: Fizmatlit, 2005)
4. Efetov K B, Tschersich A *Phys. Rev. B* **67** 174205 (2003)
5. Feigel'man M V, Ioselevich A S *JETP Lett.* **81** 277 (2005); *Pis'ma Zh. Eksp. Teor. Fiz.* **81** 341 (2005)
6. Beloborodov I S, Lopatin A V, Vinokur V M *Phys. Rev. B* **72** 125121 (2005)
7. Bartov D et al. *Phys. Rev. B* **90** 144423 (2014)
8. Mikhailovsky Yu O et al. *Solid State Phenomena* **233–234** 403 (2015)
9. Rylkov V V et al. *Phys. Rev. B* **95** 144202 (2017)
10. Milner A et al. *Phys. Rev. Lett.* **76** 475 (1996)
11. Pakhomov A B, Yan X, Zhao B *Appl. Phys. Lett.* **67** 3497 (1995)
12. Aronzon B A et al. *JETP Lett.* **70** 90 (1999); *Pis'ma Zh. Eksp. Teor. Fiz.* **70** 87 (1999)
13. Aronzon B A et al. *JETP Lett.* **71** 469 (2000); *Pis'ma Zh. Eksp. Teor. Fiz.* **71** 687 (2000)
14. Granovsky B A et al. *J. Exp. Theor. Phys.* **96** 1104 (2003); *Zh. Eksp. Teor. Fiz.* **123** 1256 (2003)
15. Gan'shina E A et al. *J. Exp. Theor. Phys.* **98** 1027 (2004); *Zh. Eksp. Teor. Fiz.* **125** 1172 (2004)
16. Bedanta S et al. *Phys. Rev. Lett.* **98** 176601 (2007)
17. Udalov O G, Beloborodov I S *J. Phys. Condens. Matter* **29** 155801 (2017)
18. Udalov O G, Beloborodov I S *Phys. Rev. B* **95** 045427 (2017)
19. Rylkov V V et al. *J. Exp. Theor. Phys.* **131** 160 (2020); *Zh. Eksp. Teor. Fiz.* **158** 164 (2020)
20. Rylkov V V et al. *J. Magn. Magn. Mater.* **459** 197 (2018)
21. Rylkov V V et al. *J. Exp. Theor. Phys.* **126** 353 (2018); *Zh. Eksp. Teor. Fiz.* **153** 424 (2018)
22. Nikolaev S N et al. *JETP Lett.* **118** 508 (2023); *Pis'ma Zh. Eksp. Teor. Fiz.* **118** 519 (2023)
23. Nikolaev S N et al. *JETP Lett.* **118** 58 (2023); *Pis'ma Zh. Eksp. Teor. Fiz.* **118** 46 (2023)
24. Mitsuyu T, Wasa K *Jpn. J. Appl. Phys.* **20** L48 (1981)
25. Drovosekov A B et al. *J. Magn. Magn. Mater.* **495** 165875 (2020)
26. Drovosekov A B et al. *JETP Lett.* **112** 84 (2020); *Pis'ma Zh. Eksp. Teor. Fiz.* **112** 88 (2020)
27. Gan'shina E A et al. *Phys. Met. Metallogr.* **24** 126 (2023); *Fiz. Met. Metalloved.* **124** 134 (2023)
28. Swamy G V et al. *AIP Advances* **3** 072129 (2013)
29. Mitani S et al. *Phys. Rev. Lett.* **81** 2799 (1998)
30. Chernoglazov K Yu et al. *Phys. Solid State* **65** 1534 (2023); *Fiz. Tverd. Tela* **65** 1602 (2023)
31. Li L et al. *Int. J. Appl. Ceram. Technol.* **16** 2047 (2019)
32. Mooij J H *Phys. Status Solidi A* **17** 521 (1973)
33. Swamy G V et al. *J. Phys. D* **48** 475002 (2015)
34. Mott N F, Davis E A *Electronic Processes in Non-Crystalline Materials* (New York: Oxford Univ. Press, 1979)
35. Shlimak I et al. *Phys. Rev. B* **55** 1303 (1997)
36. Blinov M I et al. *J. Magn. Magn. Mater.* **469** 155 (2019)
37. Nagaosa N et al. *Rev. Mod. Phys.* **82** 1539 (2010)
38. Fukumura T et al. *Jpn. J. Appl. Phys.* **46** L642 (2007)
39. Fernández-Pacheco A et al. *Phys. Rev. B* **77** 100403 (2008)
40. Onoda S, Sugimoto N, Nagaosa N *Phys. Rev. B* **77** 165103 (2008)
41. Meier H, Kharitonov M Yu, Efetov K B *Phys. Rev. B* **80** 045122 (2009)
42. Vedyayev A et al. *Phys. Rev. Lett.* **110** 247204 (2013)
43. Vedyayev A V et al. *Appl. Phys. Lett.* **103** 032406 (2013)
44. Matos-Abiague A, Fabian J *Phys. Rev. Lett.* **115** 056602 (2015)
45. Karashtin E A et al. *J. Exp. Theor. Phys.* **136** 1 (2023); *Zh. Eksp. Teor. Fiz.* **163** 5 (2023)
46. Vedyaev A V, Granovsky A B *Sov. Phys. Solid State* **28** 1293 (1986); *Fiz. Tverd. Tela* **28** 2310 (1986)
47. Liu X-J, Liu X, Sinova J *Phys. Rev. B* **84** 165304 (2011)
48. Liu X et al. *Phys. Rev. B* **83** 144421 (2011)
49. Shitade A, Nagaosa N *J. Phys. Soc. Jpn.* **81** 083704 (2012)
50. Gan'shina E A et al. *J. Exp. Theor. Phys.* **137** 572 (2023); *Zh. Eksp. Teor. Fiz.* **164** 662 (2023)